catalysts

MDPI

Article

Examination of the Catalytic Role of the Axial Cystine Ligand in the Co-Type Nitrile Hydratase from *Pseudonocardia thermophila* JCM 3095

Irene R. A. M. Ogutu [1,2], Martin St. Maurice [3], Brian Bennett [4,*] and Richard C. Holz [1,2,*]

1 Department of Chemistry, Colorado School of Mines, Golden, CO 80401, USA; iogutu@mines.edu
2 Department of Chemistry, Marquette University, P.O. Box 1881, Milwaukee, WI 53201-1881, USA
3 Department of Biology, Marquette University, 1428 W. Clybourn St., Milwaukee, WI 53201, USA; martin.stmaurice@marquette.edu
4 Department of Physics, Marquette University, 1420 W. Clybourn St., Milwaukee, WI 53201, USA
* Correspondence: brian.bennett@marquette.edu (B.B.); rholz@mines.edu (R.C.H.)

Abstract: The strictly conserved αSer162 residue in the Co-type nitrile hydratase from *Pseudonocardia thermophila* JCM 3095 (*Pt*NHase), which forms a hydrogen bond to the axial αCys108-S atom, was mutated into an Ala residue. The αSer162Ala yielded two different protein species: one was the apoform (αSer^{A}) that exhibited no observable activity, and the second (αSer^{B}) contained its full complement of cobalt ions and was active with a k_{cat} value of 63 ± 3 s^{-1} towards acrylonitrile at pH 7.5. The X-ray crystal structure of αSer^{A} was determined at 1.85 Å resolution and contained no detectable cobalt per $\alpha_2\beta_2$ heterotetramer. The axial αCys108 ligand itself was also mutated into Ser, Met, and His ligands. All three of these αCys108 mutant enzymes contained only half of the cobalt complement of wild-type *Pt*NHase, but were able to hydrate acrylonitrile with k_{cat} values of 120 ± 6, 29 ± 3, and 14 ± 1 s^{-1} for the αCys108His, Ser, and Met mutant enzymes, respectively. As all three of these mutant enzymes are catalytically competent, these data provide the first experimental evidence that transient disulfide bond formation is not catalytically essential for NHases.

Keywords: nitrile hydratase; cobalt; hydration; mutant; X-ray crystallography; UV–vis spectroscopy

Citation: Ogutu, I.R.A.M.; St. Maurice, M.; Bennett, B.; Holz, R.C. Examination of the Catalytic Role of the Axial Cystine Ligand in the Co-Type Nitrile Hydratase from *Pseudonocardia thermophila* JCM 3095. *Catalysts* **2021**, *11*, 1381. https://doi.org/10.3390/catal11111381

Academic Editor: David D. Boehr

Received: 20 October 2021
Accepted: 13 November 2021
Published: 16 November 2021

1. Introduction

Nitrile hydratases (NHases, EC 4.2.1.84) are metalloenzymes that catalyze the hydration of nitriles to their corresponding amides under ambient conditions and physiological pH [1,2]. Their biological role is not well-understood but likely involves nutrient metabolism, product biosynthesis, hormone degradation, nitrile detoxification, or nutrient assimilation [3]. NHases have attracted substantial interest as biocatalysts in preparative organic chemistry, as they can hydrate a wide range of synthetic nitrile substrates, resulting in their exploitation for biotechnological purposes as biocatalysts in the production of acrylamide and nicotinamide [4]. A key advantage of NHases is their stereoselectivity, which is particularly important in the pharmaceutical arena [5]. NHases are also useful in the bioremediation of chemical and wastewater runoff, specifically for the hydration of nitrile-based pesticides such as bromoxynil, and are thus becoming increasingly recognized as biocatalysts for green chemical processes [6]. Despite the biological, industrial, and bioremediation importance of NHase enzymes, a deeper understanding of their reaction mechanism is required to apply and exploit this elegant catalytic chemistry.

NHases contain either a low-spin Fe(III) (Fe-type) or Co(III) (Co-type) ion in their active site [7]. X-ray crystallographic studies on NHases reveal that they are $\alpha_2\beta_2$ heterotetramers with an active-site metal ion coordinated by three cysteine residues, two amide nitrogens, and a water or hydroxyl moiety (Figure 1) [7–9]. The prevailing dogma is that both the Co- and the Fe-type of $\alpha_2\beta_2$ NHase enzymes require the coexpression of an

activator (ε) protein to be fully metallated, post-translationally modified, and fully functional [10–12]. Two of the active-site cysteine residues are post-translationally modified into cysteine-sulfinic acid (–SO_2H) and cysteine-sulfenic acid (–SOH), yielding a coordination geometry termed a "claw setting"; the oxidation of equatorial Cys residues is essential for catalysis [13]. The catalytic relevance of these moieties is established, but information on their mechanistic roles is only just starting to evolve.

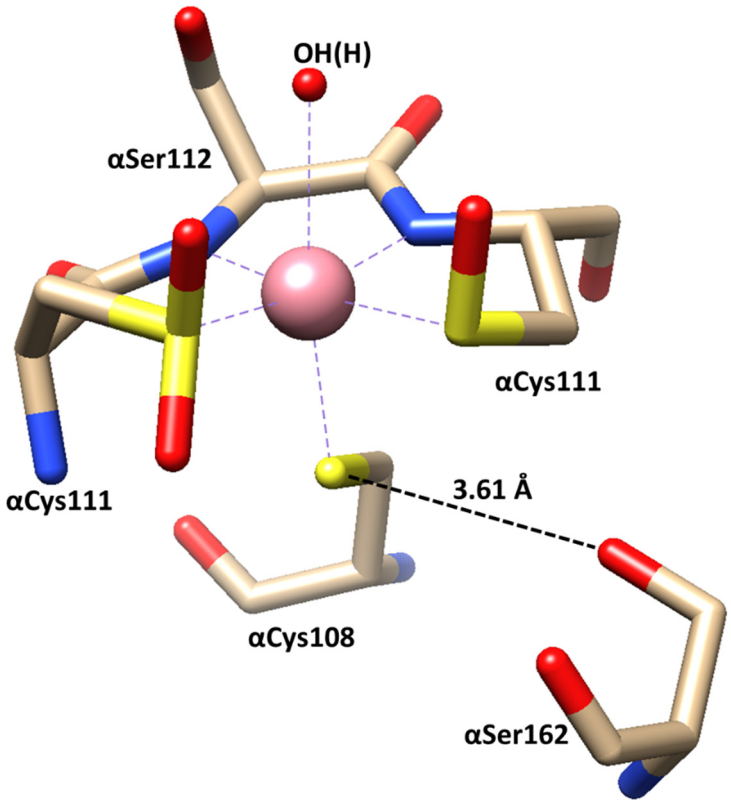

Figure 1. Active site of *Pt*NHase (PDB:1IRE). Dashed line, distance between sulfur atom of axial Cys108 ligand and oxygen atom of OH group of αSer162.

Recent theoretical studies suggested that the axial thiolate ligand can form a transient disulfide bond with a recently identified sulfenic acid cyclic intermediate (Figure 2, pathway B) [14,15]; however, a more recent theoretical study is self-inconsistent in its conclusions regarding transient disulfide formation, as the barrier for disulfide formation is similar to that of cyclic intermediate formation, suggesting that both are viable intermediates [14]. All theoretical calculations assume that the αCys ligand is a thiolate, making it a strong π-donor ligand and a good a nucleophile [14–16]. However, in NHases, the thiolate character of the αCys ligand, and hence metal ion Lewis acidity, is likely modulated through hydrogen bonding interaction, influencing the αCys sulfur ligand's π-donating ability and nucleophilicity. Sequence analysis of Co- and Fe-type NHase enzymes indicates that either an αSer or αThr residue is strictly conserved in this position, with the αSer typically found in Co-type enzymes, and the αThr found in Fe-type NHases.

To gain insight into the role of the axial αCys108 ligand in catalysis, a two-pronged approach was employed. First, the hydrogen bonding interaction between the axial αCys-S atom and a strictly conserved αSer162 residue in the Co-type NHase from *Pseudonocardia thermophila* JCM 3095 (*Pt*NHase) was investigated in substitution mutation αSer162→Ala. Thus, the H-bonding interaction, which was hypothesized to influence the αCys-S ligand's π-donating ability and nucleophilicity; hence, active-site Co(III) ion Lewis acidity was removed. Second, the axial αCys108 ligand in *Pt*NHase was substituted with Ser (αCys108Ser), Met (αCys108Met), or His (αCys108His), which significantly changes the

σ- and π-donating ability of the active-site axial ligand. Each of these mutant *Pt*NHase enzymes was analyzed via kinetic and spectrophotometric methods, and interpreted in light of an X-ray crystal structure for the αSer162Ala mutant.

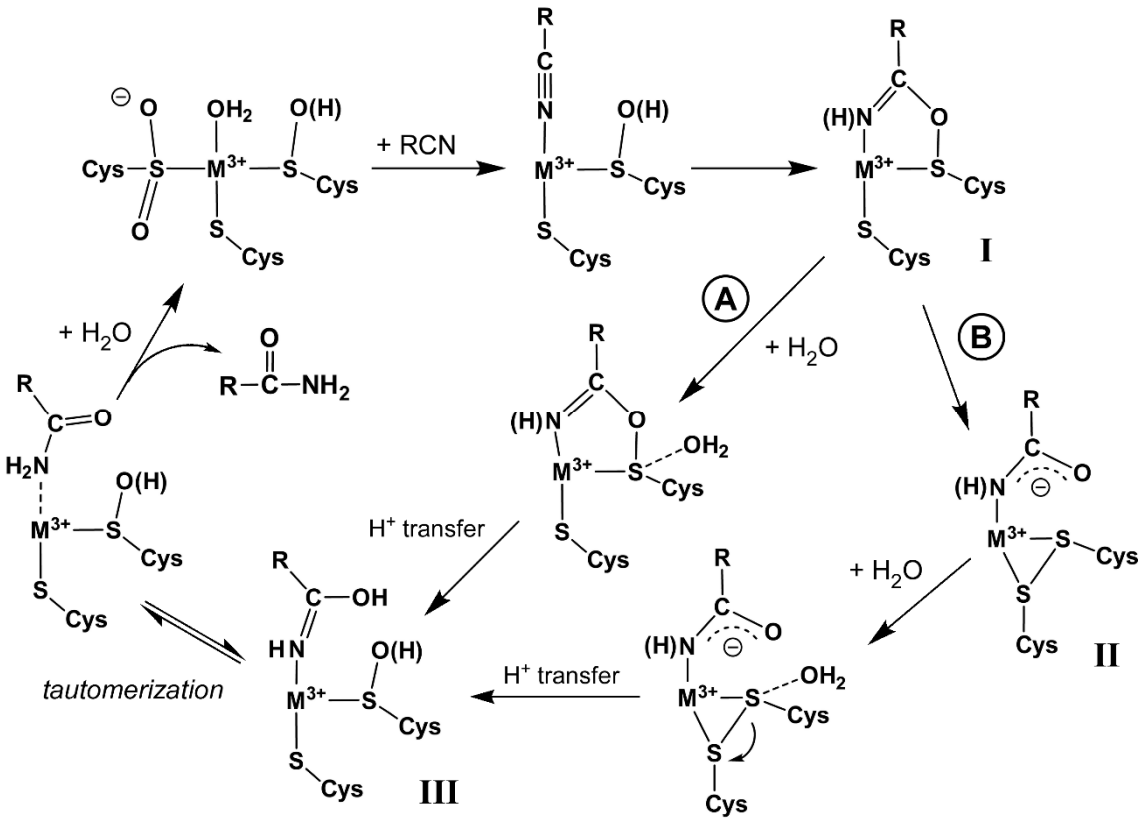

Figure 2. Proposed catalytic mechanism for NHase enzymes. Two possible pathways have been proposed and are labeled A and B. Within those pathways are several proposed intermediates of importance, which are labeled I, II, and III.

2. Results and Discussion

2.1. PtNHase αSer162Ala Mutant Enzyme: Purification and Kinetic Characterization

Initially, the αSer162Ala *Pt*NHase mutant enzyme was prepared and analyzed. The OH moiety of αSer162 is 3.6 Å from the axial αCys108 sulfur ligand and is the only group within 5 Å (Figure 1) [17,18]. Such a hydrogen bonding interaction between αSer162 and the αCys108 ligand likely influences the π-donating ability and nucleophilicity of the axial Cys ligand, which is consistent with model complex studies [19,20]. During the isolation of αSer162Ala, two species with distinct Ni^{2+} affinity chromatographic elution profiles were isolated, both of which corresponded to *Pt*NHase by sodium dodecyl sulphate-polyacrylamide gel electrophoresis(SDS-PAGE) and size-exclusion chromatography. The earlier-eluting species, termed αSer^{A}, which eluted at 150 mM imidazole, was colorless (Figure 3, vial 2) and exhibited no catalytic activity toward acrylonitrile (Table 1). The later-eluting fraction, αSer^{B}, eluted at 225 mM imidazole and was straw-colored (Figure 3, vial 3), which is similar to that of wild-type *Pt*NHase (Figure 3, vial 1). In addition, αSer^{B} was catalytically active, displaying a k_{cat} value of around 60 s^{-1}, or around 3% of the native enzyme (Table 1).

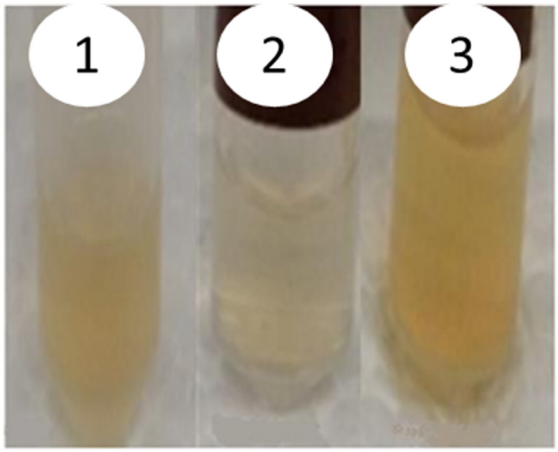

Figure 3. As purified Samples 1 (198 μM Wt-*Pt*NHase) 2 (1.1 mM *Pt*NHase αSer^{A}), and and 3 (247 μM *Pt*NHase αSer^{B}) in 50 mM HEPES pH 7.0 at room temperature.

Table 1. Kinetic constants (k_{cat} and K_m) using acrylonitrile as substrate at pH 7.5 for WT *Pt*NHase and active-site mutants.

	k_{cat} (s^{-1})	K_m (mM)	Co Content
WT *Pt*NHase	1790 ± 50	3.0 ± 0.4	1.8 ± 0.3
*Pt*NHase αSer^{A}	[a] ND	-	<0.1 ± 0.2
*Pt*NHase αSer^{B}	63.4 ± 3.2	35.0 ± 4.2	1.8 ± 0.3
*Pt*NHase αC108M	14 ± 1	3.1 ± 0.5	0.8 ± 0.2
*Pt*NHase αC108S	29 ± 3	1.8 ± 0.7	0.9 ± 0.2
*Pt*NHase αC108H	120 ± 6	2.6 ± 0.6	1.0 ± 0.2

[a] None detected.

The K_m value observed for the αSer^{B} mutant towards acrylonitrile was 35 mM, which is nearly 43-fold larger than that of WT *Pt*NHase, indicating that the loss of hydrogen bonding to the axial αCys ligand significantly diminishes the binding affinity of the nitrile substrate. This is consistent with the expected influence on the π-donating ability and nucleophilicity of the αCys ligand, and hence the Lewis acidity of the Co(III) ion. Thus, the observed diminution of substrate binding affinity could have been due to the low-spin Co(III) ion being more kinetically inert, so the axial water molecule could not dissociate, due to poorer binding affinity for the acrylonitrile substrate due to a more electron-rich low-spin Co(III) ion, or a combination of both. The presence of detectable activity in αSer^{B}–αSer162Ala indicates that, at least for a population of the αSer^{B}–αSer162Ala *Pt*NHase mutant enzyme, active-site Cys residues must be properly oxidized to cysteine sulfinic and sulfenic acids, as the oxidation of the axial Cys residues to cysteine sulfinic and sulfenic acids is required for enzymatic activity [21].

2.2. Metal Analysis and Spectral Characterization of αSer^{A} and αSer^{B} Forms of αSer162Ala Mutant Enzymes

A combination of ICP-MS and UV–vis spectroscopy was used to determine if the αSer^{A} and αSer^{B} *Pt*NHase mutant enzymes, expressed in the presence of an activator (ε) protein, contained their full complement of cobalt. As a control, ICP-MS data were obtained on WT *Pt*NHase, which revealed ~1.8 cobalt ions per $\alpha_2\beta_2$ tetramer, while the UV–vis spectrum exhibited the characteristic S → Co(III) ligand-to-metal charge-transfer (LMCT) band at ~320 nm (ε = ~29,000 M^{-1} cm^{-1}; Figure 4) that is due to the axial thiolate π to Co(III) dπ* transition [22], resulting in the observed straw color [23]. ICP-MS data obtained for the αSer^{A} and αSer^{B} forms of the αSer162Ala mutant indicated that αSer^{A} contained <0.1 cobalt ions per $\alpha_2\beta_2$ tetramer, which is the detection limit, while αSer^{B} contained ~1.8 cobalt ions per $\alpha_2\beta_2$, indistinguishable from WT *Pt*NHase (Table 1). The

UV–vis spectrum of the αSer^{B} mutant exhibited the characteristic S → Co(III) ligand-to-metal charge-transfer (LMCT) band at ~320 nm (ε = ~29,000 M^{-1} cm^{-1}), identical to WT *Pt*NHase, whereas the αSer^{A} mutant exhibited no visible absorption (Figure 4).

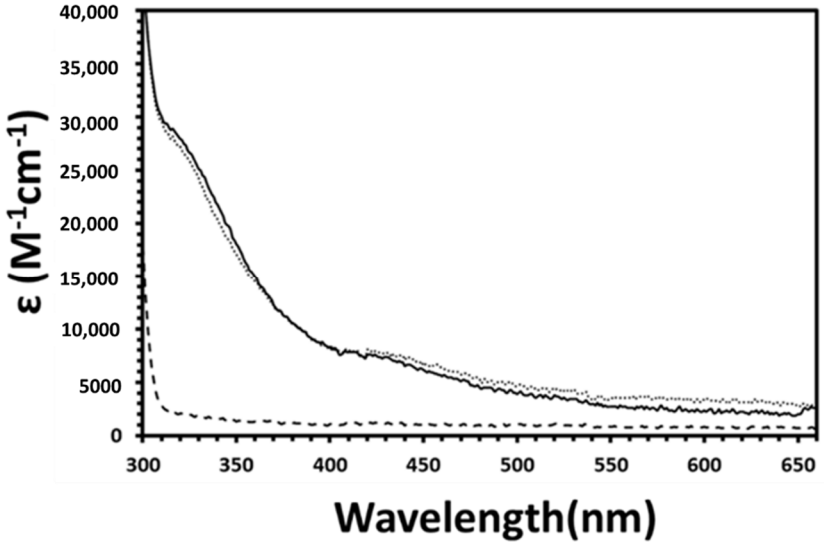

Figure 4. UV–vis absorbance spectra of 8.4 μM Wt-*Pt*NHase (solid line), 7.3 μM *Pt*NHase αSer^{A} (dotted line), and 16.2 μM *Pt*NHase αSer^{B} (dashed line) in 50 mM HEPES buffer, pH 7.0 at 25 °C.

2.3. Crystal Structure of αSer^{A} (apo-αSer162Ala) PtNHase Mutant Enzyme

Verification that the αSer^{A} form of the αSer162Ala *Pt*NHase mutant enzyme was in the apoform comes from the three-dimensional X-ray crystal structure, determined to 1.85 Å resolution (Figure 5A). While multiple attempts were made to obtain X-ray diffraction-quality crystals of the αSer^{B} mutant using a wide variety of conditions and solution/enzyme concentrations, none was successful. Details of data collection and refinement statistics for αSer^{A} are given in Table 2. The overall structure of αSer^{A} is nearly identical to that previously reported for WT *Pt*NHase (PDB code: 1IRE). On the basis of F_o–F_c difference maps (Figure 5A,B), αSer^{A} contained no detectable cobalt, as expected from ICP-AES data (Table 1). Consistent with the lack of a fully post-translationally matured metal-containing active site in the inactive αSer^{A}, the active site equatorial αCys residues were found not to be post-translationally modified to cysteine sulfinic and sulfenic acids.

The previously reported X-ray crystal structure of apo-WT *Pt*NHase that had been expressed in the absence of the activator (ε) protein (PDB code: IUGQ) indicated the presence of a disulfide bond between the axial Cys residue (αCys108) and the equatorial Cys that becomes the sulfenic acid ligand (αCys113) (Figure 5C) with an S–S bond distance of 2.04 Å [18]. In contrast, the X-ray structure of the αSer^{A} *Pt*NHase mutant enzyme, expressed in the presence of the activator (ε) protein and 0.25 mM Co(II), exhibited little or no electron density between αCys108 and αCys113 active-site residues, suggesting weak disulfide bond formation at best (Figure 5A). In addition, both the equatorial cysteine residues (αC111 and αC113) crystalized in alternate conformations, labeled A and B, with a 50:50 ratio (Figure 5B). The distance between the αCys108 and αCys113 sulfur atoms in the A and B conformations was 3.61 and 2.89 Å, respectively. Both of these distances are longer than the typical disulfide bond, and the mutual orientations of the residues in αSer^{B} are not conducive to a disulfide bond. As the orientation of αCys113 S-atom in the B conformation is identical to that of the αCys113 S-atom in the apo-WT *Pt*NHase enzyme, the lack of a disulfide bond between the αCys108 and αCys113 residues in the αSer^{A} is likely a consequence of the lack of a hydrogen bond between αSer162 and αCys108. This hydrogen-bonding interaction likely helps to preorganize αCys108 and αCys113 for disulfide bond formation in the immature active site of post-translationally unprocessed (ε^{-}) apo-WT NHase.

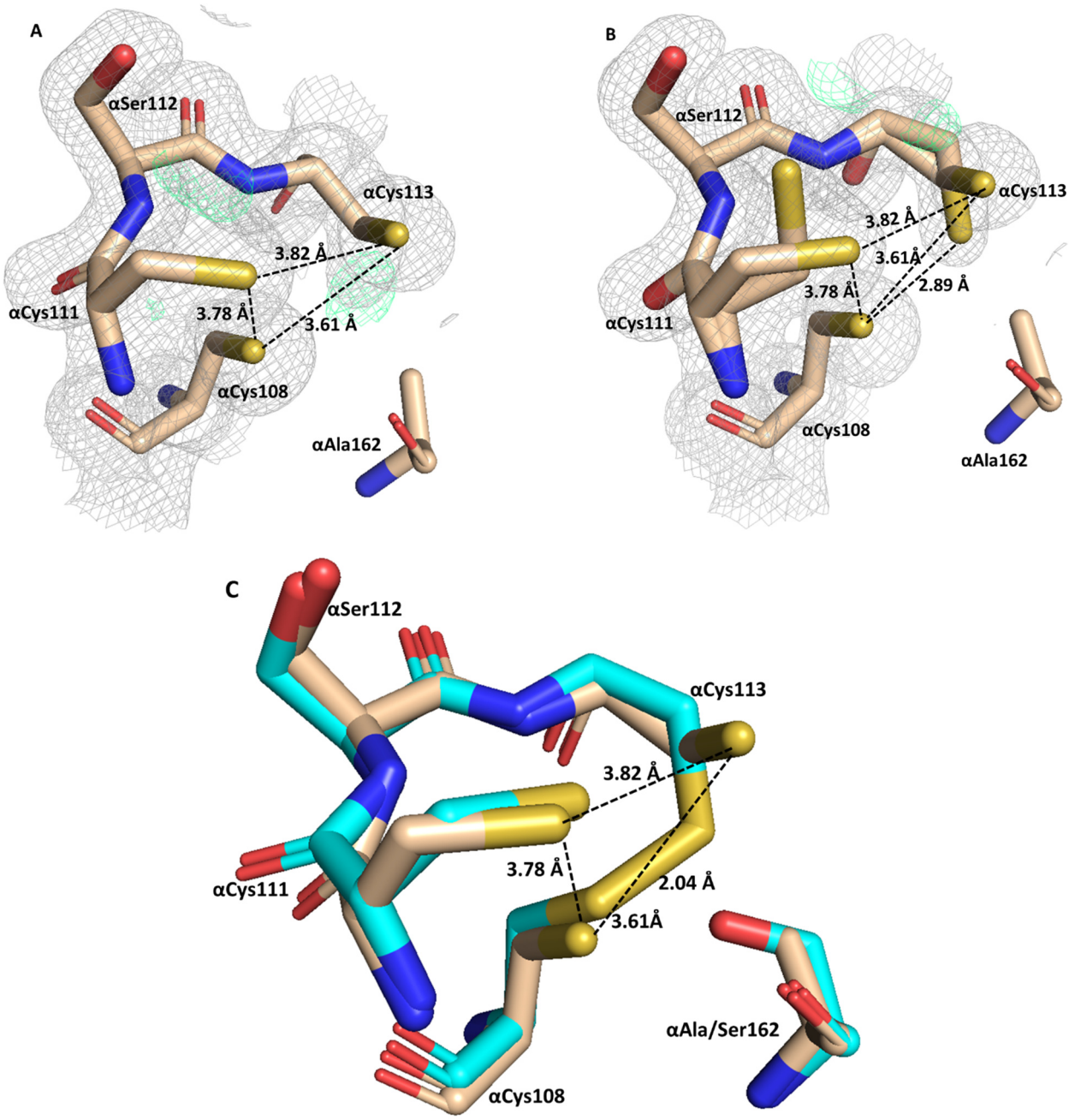

Figure 5. X-ray crystal structure of αSer^{A} at 1.8 Å resolution. (**A**) Simulated annealing omit map (2Fo–Fc) shown in gray mesh at the 1.0 σ level, contoured at 2.0 σ. Additional electron density (Fo–Fc) omit map shown as green mesh at 3.0 σ level indicating alternate αCys111 and αCys113 conformations; (PDB ID: 7SJZ) (**B**) simulated annealing omit map (2Fo–Fc) shown in gray mesh at the 1.0 σ level, contoured at 2.0 σ of αSer^{A} active site fit with both alternate conformations in a 50:50 ratio (PDB ID: 7SJZ); (**C**) superposition of active site of αSer^{A}(wheat tint) and Apo-*Pt*NHase(cyan) (PDB: 1GUQ). All bond distances shown in angstroms.

Table 2. Data collection and refinement statistics for the αSer^{A} *Pt*NHase mutant enzyme (PDB ID: 7SJZ).

PDB ID: 7SJZ	
Space group	$P3_2$ 2 1
Cell Dimensions	
α, β, γ (°)	90.0, 90.0, 120.0
a, b, c (Å)	65.91, 65.91,186.23
Resolution range (Å)	48.66–1.85 (1.92–1.85)
Redundancy	8.55 (6.84)
Completeness (%)	98.3 (98.6)
Unique reflections	40335
R_{merge}	0.055 (0.098)
Average I/σ	23.9 (12.5)
Refinement:	
Resolution range (Å)	42.05–1.85
R_{work}	0.164 (0.172)
R_{free}	0.211 (0.218)
Number of nonsolvent atoms	3447
Number of water molecules	516
Wilson B values (Å^2)	17.7
Average B factor	18.7
Protein	17.4
Solvent	28.5
Ramachandran (%)	
Favored	98.3
Allowed	1.7
Disallowed	0.0
Outlier (%)	0.0
r m s bond deviations	
Bond length (Å)	0.011
Bond angle (°)	1.642

2.4. PtNHase αCys108Ser, αCys108Met, and αCys108His Mutant Enzymes: Purification and Kinetic Characterization

The expression of *Pt*NHase αCys108Ser, αCys108Met, and αCys108His, in the presence of Co(II) but in the absence of the (ε) activator protein, provided colorless species in each case. In contrast, when expressed in the presence of activator (ε) protein, the enzymes exhibited color indicative of cobalt ion complexation (Figure 6). SDS-PAGE analysis revealed that each mutant enzyme was >95% pure (Figure S1). The αCys108Ser *Pt*NHase exhibited a faint green color (0.16 mM) at pH 7.5 (Figure 6, Vial 2) in contrast to the straw-colored WT *Pt*NHase enzyme. αCys108Met *Pt*NHase (0.12 mM) exhibited a lime green color, whereas αCys108His *Pt*NHase (0.5 mM) exhibited a light pink color. All the *Pt*NHase αCys108Ser, αCys108Met, and αCys108His enzymes were catalytically active. αCys108His was the most active of the Cys108-substituted variants, with a k_{cat} of 120 s^{-1}, or ~7% of WT *Pt*NHase, and a K_m of ~2.5 mM, a value indistinguishable from that of WT *Pt*NHase (Table 1). αCys108Ser exhibited a k_{cat} of ~30 s^{-1} or ~2% of WT *Pt*NHase and a K_m value of ~2 mM while αCys108Met was the least active of the three axial mutants, with a k_{cat} of ~15 s^{-1} or ~1% of the activity observed for WT *Pt*NHase with a K_m value of ~3 mM (Table 1). That each of these axial αCys ligand mutants are catalytically active definitively indicates that the formation of a transient disulfide bond between the axial αCys108 ligand and the equatorial sulfenic acid ligand, αCys113, is not catalytically required. While such an interaction may occur in the WT enzyme to facilitate catalysis, it is not an essential catalytic step for NHase activity.

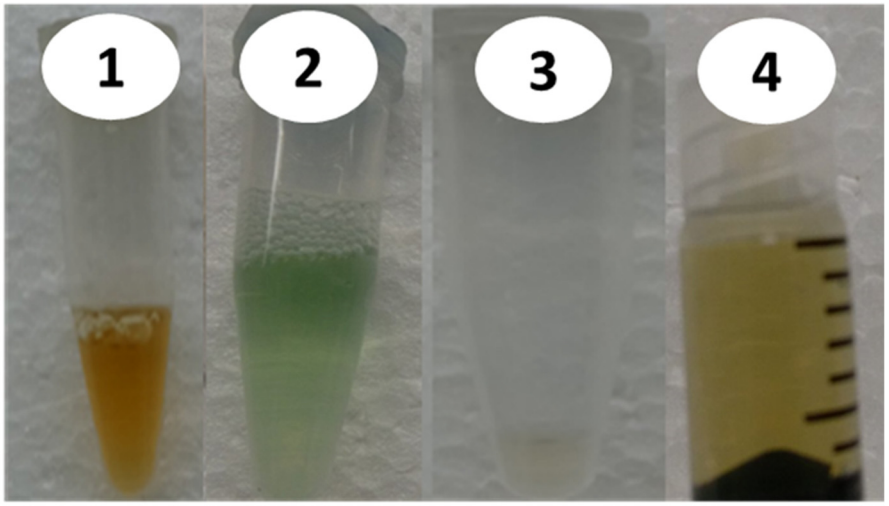

Figure 6. *Pt*NHase in 50 mM HEPES pH 7.0 buffer at room temperature; (1) 0.54 mM *Pt*NHase WT, (2) 0.16 mM *Pt*NHase αCys108Ser, (3) 0.50 mM *Pt*NHase αCys108His, (4) 0.43 mM *Pt*NHase αCys108Met.

The order of catalytic rates for the WT and each *Pt*NHase axial αCys ligand mutant is WT >>> His > Ser > Met, which is consistent with the expected σ- and π-donating ability of each ligand. Histidine is a strong σ-donor, but unlike the native αCys ligand, it cannot participate in π-donation. On the other hand, serine and methionine are weak σ-donors and weak π-donor ligands, with Met being the poorer ligand of the two, as it is a softer base. These data are consistent with NHase biomimetic model complex studies that revealed that the axial thiolate increases the ligand exchange rate, since substituting the trans-thiolate with a nitrogen ligand decreased the exchange rate by three orders of magnitude [19,20]. Similar to heme systems [24], it was proposed that the axial thiolate group in NHase enzymes "pushes" electron density, modulating the Lewis acidity of the active site metal ion, and assisting the active-site trivalent metal ion to bind and activate nitriles.

2.5. Metal Analysis and Spectrophotometric Characterization of αCys108Ser, αCys108Met, and αCys108His Mutant Enzymes

A combination of ICP-MS and UV–vis spectroscopy was used to determine if the αCys108Ser, αCys108Met, and αCys108His *Pt*NHase mutant enzymes expressed in the presence of an activator (ε) protein contained their full complement of cobalt. ICP-MS data obtained for the αCys108Ser, αCys108Met, and αCys108His mutants indicated that each contained ~1 cobalt ion per $\alpha_2\beta_2$ tetramer, which is about half of that observed for WT *Pt*NHase (~1.8 cobalt) per $\alpha_2\beta_2$ tetramer (Table 1). The lower activity observed for each mutant *Pt*NHase enzyme must, therefore, be partially due to the diminished complement of cobalt in the active site. Moreover, it appears that the electron donating ability of the axial ligand plays a role in the insertion of the metal ion into the active site. The UV–vis spectrum of αCys108Ser exhibited red-shifted S → Co(III) LMCT bands at ~430 (ε = ~3000 M^{-1} cm^{-1}) and ~620 nm (ε = ~2000 M^{-1} cm^{-1}) while αCys108Met, and αCys108His mutant enzymes also exhibited red shifted S → Co(III) LMCT bands at ~350 (ε = ~2000 M^{-1} cm^{-1}) and ~550 nm (ε = ~800 M^{-1} cm^{-1}) (Figure 7). For WT *Pt*NHase, the observed S → Co(III) LMCT bands are observed between 310 and 450 nm and are characteristic of strong π-electron donation from the axial thiolate ligand to the low-spin Co(III) ion [25–27]. The red-shifted S → Co(III) LMCT bands observed for the αCys108Ser, αCys108Met, and αCys108His mutants can be attributed to the poorer electron donating ability, particularly weak or no π-donating ability of the axial ligand, resulting in an increase in Lewis acidity of the active site Co(III) ion. These data clearly show that the axial αCys108 plays a significant catalytic role by tuning the Lewis acidity of the active site low-spin Co(III) ion, which regulates the axial water exchange rate and substrate binding ability.

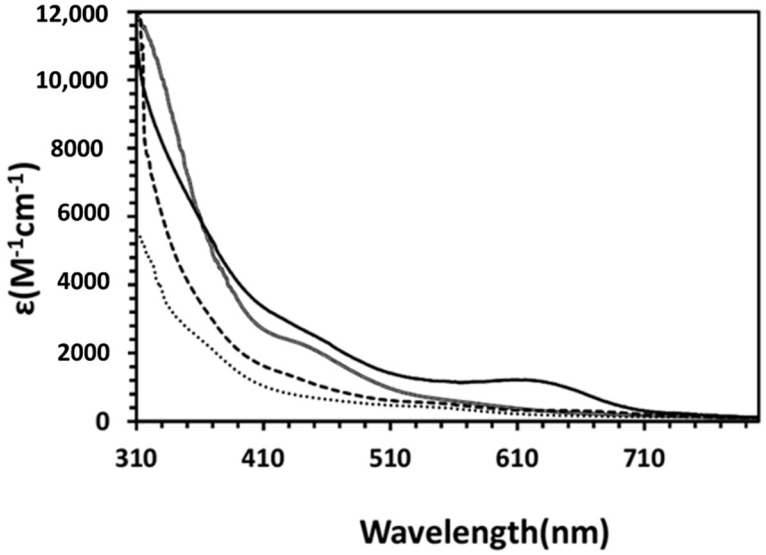

Figure 7. UV–vis absorbance spectra of the *Pt*NHase (compound) wildtype, (solid) αCys108Ser, (dashed) αCys108His, and (dotted) αCys108Met in 50 mM HEPES pH 7.0 at 25 °C.

3. Material and Methods

3.1. Materials

All reagents were commercially purchased and were of the highest available purity. Isopropyl-β-D-1-thiogalactopyranoside (IPTG), tris(2-carboxyethyl)phosphine (TCEP), N-2-hydroxyethylpiperazine-N-2-ethane sulfonic acid (HEPES), acrylonitrile, methacrylonitrile, acetonitrile, Luria-Bertani (LB) powder, sodium chloride (NaCl), and butyric acid were purchased from either Sigma-Aldrich or Fisher scientific. NEB and BL21(DE3) competent cells were obtained from Agilent Technologies, and plasmid purification kits were purchased from Promega.

3.2. Mutagenesis

The gene sequence encoding the β- and α-subunits of *Pt*NHase was inserted into a pET-28a+ vector between HindIII and NcoI cloning sites with a six-histidine tag on the α-subunit. The nucleic acid sequence of the pET28a$^+$ plasmid carrying the wild-type *Pt*NHase α- and β-subunits was used for mutagenic primer design (*1*) using ApE software, and oligonucleotides were obtained from Integrated DNA Technologies Inc. The forward primer sequences used for mutagenesis are listed below, and the reverse primers had complementary sequences to those of their corresponding forward primer.

- 5′GGAGATCAAGGTCTGGGACgccAGCTCCGAGATCC3′ *Pt*NHase αS162A
- 5′CCACGTCGTCGTGatgACGCTCTGCTCCTGC 3′ *Pt*NHase αC108M
- 5′CGTCGTCGTGcaCACGCTCTGCTCCTGC 3′ *Pt*NHase αC108H
- 5′CCACGTCGTCGTGaGCACGCTCTGCTC-3′ *Pt*NHase αC108S

The changed bases are in lower case, and reverse primers were of a similar base length. Polymerase chain reaction was performed, and the resulting mutant genes were inserted into the pET28a$^+$ plasmid. Each mutant plasmid was prepared using a QuickChange site-directed mutagenesis kit (Agilent) via the polymerase chain reaction (PCR). Two PCR half reaction mixtures were separately prepared with forward and reverse PCR primers. Mutant plasmids were transformed into *XL10-Gold* Ultracompetent cells to produce multiple copies and these cells were grown overnight in LB media. Plasmids were purified using a Promega Wizard SV genomic DNA purification kit according to the manufacturer's protocol, and the mutation was confirmed by sequencing (Functional Biosciences, Madison, WI, USA).

3.3. Transformation, Growth, Harvesting, and Storage

The plasmid containing the β and α subunits (pET-28a+ vector), and that of the corresponding activator genes in pET-21a+ were cotransformed into BL21(DE3) *E. coli* cells for the expression. Cells for these separate expressions systems were grown on an LB agar plate containing kanamycin (50 μg/mL) and ampicillin (100 μg/mL), and incubated overnight at 37 °C. A single colony was used to inoculate separate 50 mL flasks of LB Miller culture containing kanamycin (50 μg/mL) and ampicillin (100 μg/mL), and allowed to grow overnight at 37 °C with constant shaking. These cultures were used to inoculate 6 L of LB Miller culture containing kanamycin (50 μg/mL) and ampicillin (100 μg/mL). Cells were grown at 37 °C with constant shaking until an optical density of ~0.8–1.0 at 600 nm had been reached. The culture was cooled to 20 °C and induced with 0.1 mM isopropyl-β-D-1-thiogalactopyranoside (IPTG). The culture was supplemented with 0.25 mM cobalt chloride and shaken for an additional 16 h at 18 °C. Cells expressing the mutant enzymes were pelleted by centrifugation at 5000× *g* for 10 min and resuspended in 50 mM HEPES at pH 7.5. The cell paste was stored at −80 °C until needed.

3.4. Purification of WT/Mutant PtNHase

A series of buffers were prepared for the purification of each *Pt*NHase mutant enzyme. Components and pH values of buffers were (A) 50 mM NaH_2PO_4, 500 mM NaCl and 10 mM imidazole, pH 7.5; (B) 50 mM NaH_2PO_4, 500 mM NaCl and 500 mM imidazole, pH 7.5; and (C) 50 mM HEPES, 300 mM NaCl, pH 7.5. Cells expressing each mutant enzyme were lysed by ultrasonication (Misonix Sonicator 3000) in 30 s increments for 12 min at 21 W on ice. The cell lysate was separated from cell debris by centrifugation for 40 min at 10,000× *g*. The supernatant was loaded onto a pre-equilibrated IMAC Ni-NTA column and washed with 20 column volumes of buffer A with 3% buffer B. Each mutant enzyme was eluted using a buffer B gradient. The fractions for each enzyme sample were pooled together, concentrated, and loaded on HiLoad 16/600 Superdex 200 pg size exclusion column and eluted using buffer C. The fractions of the enzymes were pooled together, concentrated, and buffer-exchanged into 50 mM HEPES at pH 7.0. The purity of each enzyme was characterized by SDS-PAGE (Figure S1).

3.5. Steady-State Kinetic Assays

The enzymatic activity of the *Pt*NHase mutant enzymes towards the substrate acrylonitrile (acrylamide; $\Delta\varepsilon_{225}$ = 2.9 mM^{-1} cm^{-1}) was measured by following product formation using a Shimadzu UV-2450 spectrophotometer equipped with a TCC temperature controller (Tables 1 and 2). A 1 mL reaction mixture was prepared in 50 mM Tris-HCl pH 7.5 at 25 °C. The assay concentrations of acrylonitrile were 1–100 mM with enzyme concentrations ranging from 100 to 200 nM. Kinetic constants V_{max} and K_m were calculated by fitting the data to the Michaelis and Menten equation using OriginPro 9.0 software (OriginLab, Northampton, MA, USA) (Figure S2). One unit of enzyme activity was defined as the amount of enzyme that catalyzed the production of 1 μmol of product per minute at 25 °C.

3.6. Metal Analysis and UV–Vis Spectroscopy

The metal content of each *Pt*NHase mutant enzyme and wild-type *Pt*NHase was obtained using inductively coupled plasma mass spectrometry (ICP-MS) at the Water Quality Center in the College of Engineering at Marquette University (Milwaukee, WI, USA). Each enzyme sample was denatured using 2 mL of 8 M urea, followed by the addition of a 0.2% nitric acid and 5% hydrochloric acid *v*/*v* mixture to a final volume of 10 mL. These samples were incubated for 3 h at room temperature to ensure complete acid digestion. Digested protein samples were centrifuged to remove precipitated protein and filtered using 0.2 μm filter. UV–vis spectra of WT and each mutant *Pt*NHase enzyme were obtained in 50 mM HEPES buffer, pH 7.0 at 25 °C in a 1 cm quartz cuvette on a Shimadzu UV-2600 spectrophotometer equipped with a TCC-240A temperature-controlled cell holder.

3.7. Crystallization and Data Collection of apo-PtNHase αSer162Ala

Crystallization of the nearly colorless *Pt*NHase αSer162Ala mutant enzyme was performed following the previously reported protocol with slight modifications in the precipitant concentration [23]. A 1.2 M sodium citrate tribasic in 0.1 M HEPES buffer at pH 7.0 was used instead of the standard 1.4 M sodium citrate tribasic concentration. Diffraction quality crystals grew within two weeks and belonged to the space group $P3_221$ with one copy of heterodimer in the asymmetric unit. Crystallographic data were collected at 100 K using a home source rotating anode Rigaku MicroMax-007 HF X-ray diffractometer at a wavelength of 1.54 Å. All data were indexed, integrated, merged and scaled using HKL2000.4 [28]. Crystal parameters, data collection, and processing statistics are given in Table 3. Phasing was carried out with molecular replacement using the Phaser program from the CCP4 software suite. The structure of wild-type *Pt*NHase (PDB code 1IRE) [17] without any water molecules and ligands except for the cobalt ion was used as the starting search model. Initial R and R_{free} and were 0.183 and 0.228, respectively. Rigid body refinement was followed by restrained refinement with Refmac55 [29], and further manual model inspection and adjustments with Coot.6 [30]. When converged refinement, solvent molecules were added over several rounds, providing R and R_{free} values of 0.162 and 0.207, respectively.

Table 3. Selected bond distances.

Crystal ID	Atom1	Atom2	Length (Å)
*Pt*NHase^{WT} (PDB: 1IRE)	αCSY108(SG)	αCSD111(SG)	3.28
	αCSO113(SG)	αCSD111(SG)	3.16
	αCSY108(SG)	αCSO113(SG)	3.09
*Apo-Pt*NHase^{WT} (PDB: 1UGQ)	αCYS108(SG)	αCYS111(SG)	3.27
	αCYS113(SG)	αCYS111(SG)	4.28
	αCYS108(SG)	αCYS113(SG)	2.03
*Pt*NHase αSer^{A}	αCYS108(SG)	αCSD111(SG)A	3.68
	αCSO113(SG)	αCSD111(SG)A	3.81
	αCSO113(SG)	αCYS108(SG)	3.61
	αCYS108(SG)	αCSO113(SG)B	3.89
	αCYS108(SG)	αCSD111(SG)B	5.05

4. Conclusions

Four *Pt*NHase mutant enzymes, namely, Ser162Ala, αCys108Ser, αCys108Met, and αCys108His, which target the axial αCys108 ligand were reported. As each of these mutants are catalytically active, these data provide the first experimental evidence that transient disulfide bond formation is not catalytically essential for NHases (Figure 2, pathway B), a key mechanistic piece of information. While the formation of a transient disulfide bond in the transition state of catalysis is clearly not required, it is certainly possible in the WT enzyme. However, theoretical studies showed that the diminution of activity in these NHase variants that lack the ability to form a disulfide bridge may correspond to only a few (2–3) kCal/mol, a value that is close even to the 1.7 kCal/mol available from thermal excitation at 25 °C [14,15]. Given the inherent uncertainty in such calculations, the role of a disulfide in the native reaction is still essentially a matter of speculation until definitive experimental evidence becomes available.

The data here are consistent with NHase model complex data, insofar as they revealed that an axial thiolate residue increases the ligand exchange rate. Substitution of the trans-thiolate with a nitrogen ligand decreases the exchange rate by three orders of magnitude [19,20]. Similar to heme systems [24], the axial thiolate group in NHase enzymes may "push" electrons, assisting the active-site trivalent metal ion to bind and activate nitriles. As such, the cysteinate trans effect appears to play a role in substrate binding and activation of the CN triple bond, and aid in the dissociation of the amide product. Combinations

of these data indicate that the axial αCys108 ligand's primary catalytic role is to provide electron density to the active-site metal ion to tune its Lewis acidity, thus decreasing the ligand exchange rate.

Supplementary Materials: The following are available online at https://www.mdpi.com/article/10.3390/catal11111381/s1, Figure S1: SDS-PAGE for the purified *Pt*NHase wildtype and mutants, Figure S2: Michaelis-Menten graphs for *Pt*NHase protein samples.

Author Contributions: I.R.A.M.O. prepared expression plasmids, carried out protein expression, purification, and enzymatic assays, prepared samples for metal and spectroscopic analysis, grew crystals, and analyzed the results. M.S.M. collected X-ray data and solved the structure with I.R.A.M.O., R.C.H. and B.B. conceived of the idea and wrote the paper with I.R.A.M.O. and M.S.M. All authors have read and agreed to the published version of the manuscript.

Funding: This work was supported by the National Science Foundation (CHE-1808711, R.C.H. and B.B.; CHE-1532168 B.B. and R.C.H.), the Todd Wehr Foundation, and Bruker Biospin.

Conflicts of Interest: The authors declare no conflict of interest.

References

1. Yamada, H.; Kobayashi, M. Nitrile hydratase and its application to industrial production of acrylamide. *Biosci. Biotechnol. Biochem.* **1996**, *60*, 1391–1400. [CrossRef]
2. Brady, D.; Beeton, A.; Zeevaart, J.; Kgaje, C.; Rantwijk, F.; Sheldon, R.A. Characterisation of nitrilase and nitrile hydratase biocatalytic systems. *Appl. Microbiol. Biotechnol.* **2004**, *64*, 76–85. [CrossRef]
3. Howden, A.J.; Preston, G.M. Nitrilase enzymes and their role in plant-microbe interactions. *Microb. Biotechnol.* **2009**, *2*, 441–451. [CrossRef]
4. Mathew, C.; Nagasawa, T.; Kobayashi, M.; Yamada, H. Nitrilase catalyzed production of nicotinic acid from 3-cyanopyridine in *Rhodococcus rhodochrous* J1. *Appl. Environ. Microbiol.* **1988**, *54*, 1030–1032. [CrossRef] [PubMed]
5. Mylerova, V.; Martinkova, L. Synthetic applications of nitrile-converting enzymes. *Curr. Org. Chem.* **2003**, *7*, 1279–1295. [CrossRef]
6. Baxter, J.; Cummings, S.P. The current and future applications of microorganism in the bioremediation of cyanide contamination. *Antonie Leeuwenhoek* **2006**, *90*, 1–17. [CrossRef]
7. Kovacs, J.A. Synthetic analogues of cysteinate-ligated non-heme iron and non-corrinoid cobalt enzymes. *Chem. Rev.* **2004**, *104*, 825–848. [CrossRef]
8. Harrop, T.C.; Mascharak, P.K. Fe(III) and Co(III) centers with carboxamido nitrogen and modified sulfur coordination: Lessons learned from nitrile hydratase. *Acc. Chem. Res.* **2004**, *37*, 253–260. [CrossRef] [PubMed]
9. Jin, H.; Turner, J.I.M.; Nelson, M.J.; Gurbiel, R.J.; Doan, P.E.; Hoffman, B.M. Coordination Sphere of the Ferric Ion in Nitrile Hydratase'. *J. Am. Chem. Soc.* **1993**, *115*, 5290–5291. [CrossRef]
10. Nishiyama, M.; Horinouchi, S.; Kobayashi, M.; Nagasawa, T.; Yamada, H.; Beppu, T. Cloning and characterization of genes responsible for metabolism of nitrile compounds from Pseudomonas chlororaphis B23. *J. Bacteriol.* **1991**, *173*, 2465–2472. [CrossRef] [PubMed]
11. Hashimoto, Y.N.M.; Horinouchi, S.; Beppu, T. Nitrile hydratase gene from Rhodococcus sp. N-774 requirement for its downstream region for efficient expression. *Biosci. Biotechnol. Biochem.* **1994**, *58*, 1859–1869. [CrossRef] [PubMed]
12. Nojiri, M.; Yohda, M.; Odaka, M.; Matsushita, Y.; Tsujimura, M.; Yoshida, T.; Dohmae, N.; Takio, K.; Endo, I. Functional Expression of Nitrile Hydratase in Escherichia coli: Requirement of a Nitrile Hydratase Activator and Post-Translational Modification of a Ligand Cysteine. *J. Biochem.* **1999**, *125*, 696–704. [CrossRef]
13. Tsujimura, M.; Odaka, M.; Nakayama, H.; Dohmae, N.; Koshino, H.; Asami, T.; Hoshino, M.; Takio, K.; Yoshida, S.; Maeda, M.; et al. A novel inhibitor for Fe-type nitrile hydratase: 2-cyano-2-propyl hydroperoxide. *J. Am. Chem. Soc.* **2003**, *125*, 11532–11538. [CrossRef] [PubMed]
14. Light, K.M.; Yamanaka, Y.; Odaka, M.; Solomon, E.I. Spectroscopic and Computational Studies of Nitrile Hydratase: Insights into Geometric and Electronic Structure and the Mechanism of Amide Synthesis. *Chem. Sci. (R. Soc. Chem. 2010)* **2015**, *6*, 6280–6294. [CrossRef]
15. Hopmann, K.H. Full Reaction Mechanism of Nitrile Hydratase: A Cyclic Intermediate and an Unexpected Disulfide Switch. *Inorg. Chem.* **2014**, *53*, 2760–2762. [CrossRef]
16. Kayanuma, M.; Shoji, M.; Yohda, M.; Odaka, M.; Shigeta, Y. Catalytic Mechanism of Nitrile Hydratase Subsequent to Cyclic Intermediate Formation: A QM/MM Study. *J. Phys. Chem. B* **2016**, *120*, 3259–3266. [CrossRef]
17. Miyanaga, A.; Fushinobu, S.; Ito, K.; Wakagi, T. Crystal structure of cobalt-containing nitrile hydratase. *Biochem. Biophys. Res. Commun.* **2001**, *288*, 1169–1174. [CrossRef] [PubMed]
18. Miyanaga, A.; Fushinobu, S.; Ito, K.; Shoun, H.; Wakagi, T. Mutational and structural analysis of cobalt-containing nitrile hydratase on substrate and metal binding. *Eur. J. Biochem.* **2004**, *271*, 429–438. [CrossRef]

19. Shearer, J.; Jackson, H.L.; Schweitzer, D.; Rittenberg, D.K.; Leavy, T.M.; Kaminsky, W.; Scarrow, R.C.; Kovacs, J.A. The first example of a nitrile hydratase model complex that reversibly binds nitriles. *J. Am. Chem. Soc.* **2002**, *124*, 11417–11428. [CrossRef] [PubMed]
20. Shearer, J.; Kung, I.Y.; Lovell, S.; Kaminsky, W.; Kovacs, J.A. Why is there an "inert" metal center in the active site of nitrile hydratase? Reactivity and ligand dissociation from a five-coordinate Co(III) nitrile hydratase model. *J. Am. Chem. Soc.* **2001**, *123*, 463–468. [CrossRef]
21. Arakawa, T.; Kawano, Y.; Katayama, Y.; Nakayama, H.; Dohmae, N.; Yohda, M.; Odaka, M. Structural Basis for Catalytic Activation of Thiocyanate Hydrolase Involving Metal-Ligated Cysteine Modification. *J. Am. Chem. Soc.* **2009**, *131*, 14838–14843. [CrossRef] [PubMed]
22. Martinez, S.; Yang, X.H.; Bennett, B.; Holz, R.C. A cobalt-containing eukaryotic nitrile hydratase. *BBA-Proteins Proteom* **2017**, *1865*, 107–112. [CrossRef] [PubMed]
23. Martinez, S.; Wu, R.; Sanishvili, R.; Liu, D.; Holz, R. The Active Site Sulfenic Acid Ligand in Nitrile Hydratases Can Function as a Nucleophile. *J. Am. Chem. Soc.* **2014**, *136*, 1186–1189. [CrossRef]
24. Vetter, S.W.; Terentis, A.C.; Osborne, R.L.; Dawson, J.H.; Goodin, D.B. Replacement of the axial histidine heme ligand with cysteine in nitrophorin 1: Spectroscopic and crystallographic characterization. *J. Bio. Inorg. Chem.* **2009**, *14*, 179–191. [CrossRef]
25. Lugo-Mas, P.; Dey, A.; Xu, L.; Davin, S.D.; Benedict, J.; Kaminsky, W.; Hodgson, K.O.; Hedman, B.; Solomon, E.I.; Kovacs, J.A. How does single oxygen atom addition affect the properties of an Fe-nitrile hydratase analogue? The compensatory role of the unmodified thiolate. *J. Am. Chem. Soc.* **2006**, *128*, 11211–11221. [CrossRef]
26. Yamanaka, Y.; Hashimoto, K.; Ohtaki, A.; Noguchi, K.; Yohda, M.; Odaka, M. Kinetic and structural studies on roles of the serine ligand and a strictly conserved tyrosine residue in nitrile hydratase. *J. Biol. Inorg. Chem.* **2010**, *15*, 655–665. [CrossRef]
27. Odaka, M.; Kohda, D.; Lax, I.; Schlessinger, J.; Inagaki, F. Ligand-binding enhances the affinity of dimerization of the extracellular domain of the epidermal growth factor receptor. *J. Biochem.* **1997**, *122*, 116–121. [CrossRef] [PubMed]
28. Otwinowski, Z.; Minor, W. Processing of X-ray diffraction data collected in oscillation mode. *Methods Enzymol.* **1997**, *276*, 307–326.
29. Murshudov, G.N.; Vagin, A.A.; Dodson, E.J. Refinement of macromolecular structures by the maximum-likelihood method. *Acta Crystallogr. D Biol. Crystallogr.* **1997**, *53*, 240–255. [CrossRef]
30. Emsley, P.; Cowtan, K. Coot: Model-building tools for molecular graphics. *Acta Crystallogr. D Biol. Crystallogr.* **2004**, *60*, 2126–2132. [CrossRef]